Construction and Building Materials 223 (2019) 679–691

Contents lists available at ScienceDirect

Construction and Building Materials

journal homepage: www.elsevier.com/locate/conbuildmat

Failure analytical model of reinforced concrete slab under impact loading

Xiangzhao Xu, Tianbao Ma, Jianguo Ning *

State Key Laboratory of Explosion Science and Technology, Beijing Institute of Technology, Beijing 100081, China

HIGHLIGHTS

- Failure analytical model of reinforced concrete under impact loading is developed.
- Experiments of projectile perforation of reinforced concrete slabs were performed.
- Results predicted by the analytical model agreed closely with experimental data.
- Effects of analytical model parameters on perforation performance were discussed.

GRAPHICAL ABSTRACT

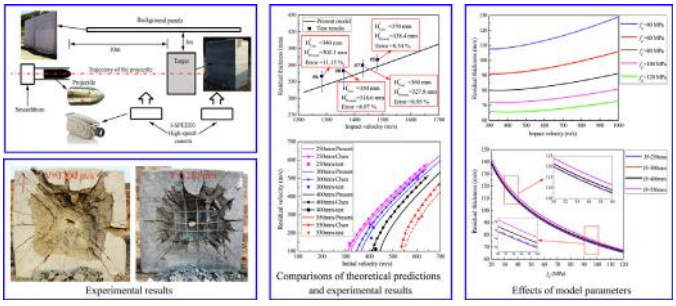

ARTICLE INFO

Article history:
Received 4 May 2019
Received in revised form 1 July 2019
Accepted 2 July 2019

Keywords:
Reinforced concrete
Perforation
Energy method
Failure characteristic

ABSTRACT

A failure analytical model was developed to assess the characteristics of reinforced concrete slabs under oblique perforation by a rigid projectile in three stages: initial cratering, tunneling and shear plugging. The energy dissipation for the initial cratering and tunneling was obtained by integrating the axial resistance force along the penetration direction, and for shear plugging using a new method considering the reinforcement. Analytical expressions for the failure characteristics of reinforced concrete slabs were obtained using energy methods. Projectile perforation experiments were conducted for thick concrete and reinforced concretes slabs and the damage size was measured. The theoretical predictions closely agreed with the experimental results and a parametric analysis of the slab failure characteristics were also discussed.

1. Introduction

Concrete and reinforced concrete have been widely used in various defense and civil engineering fields for anti-impact protection of structures, such as bridges, dams, and nuclear power plants, against high dynamic impact loading [1–3]. Hence, understanding the failure characteristics of a reinforced concrete slab under such impact loading is crucial [4,5]. For example, several concrete fragments that will cause serious secondary damage to the facilities inside the protective structure will be generated on the rear face of a reinforced concrete slab when a high-speed projectile perforates it [6–9]. Therefore, research into projectile penetration or perforation of high-value buildings and structures has been receiving considerable attention.

Extensive experimental research on projectile penetration and perforation of a concrete slab has been conducted over the last century, and several penetration and perforation empirical formulas have been obtained [10,11], such as the widely used Petry, ACE, Barr (UKAEA), and NDRC formulas. Although many experiments have been concerned with the penetration of reinforced concrete slabs, the effect of reinforcing bars has been incorporated only in some formulas, such as the Petry, Barr (UKAEA), and Boswell formulas [12]. In particular, Forrestal et al. developed a rigid elastic

* Corresponding author.
E-mail address: jgning@bit.edu.cn (J. Ning).

https://doi.org/10.1016/j.conbuildmat.2019.07.008
0950-0618/

dynamics model based on dynamic spherical and cylindrical cavity expansion, which was successfully applied to the penetration of concrete, rock, and soil mediums [13–18]. Based on the research of Forrestal et al. [13,14], Chen and Li [19,20] subsequently proposed two dimensionless parameters, projectile impact condition and projectile geometry, to describe the process of a rigid projectile penetrating into a concrete slab. Based on this, Chen et al. [21] further proposed a model containing three-stage: initial cratering, tunneling and shear plugging; thus, describing projectile perforation of a concrete slab.

Reinforcing bars significantly influence the integral penetration resistance of reinforced concrete [17,20], as they provide geometric constraints on the concrete being crushed, which may affect the size and distribution of such plastic deformation zones. Reinforcing bars also have similar constraints for concrete slabs subjected to high dynamic impact loading. However, considering the effects of reinforcing bars in theoretical modeling is a challenging problem. Consequently, the reinforcing bars or their effect on the theoretical penetration models of reinforced concrete slabs are not extensively considered [13,22]. Approximation methods have been employed by treating the reinforced concrete equivalent to only strength-enhanced concrete or to sandwich structures of stacked concrete and thin steel plates. However, only a few studies have considered the specific effects of reinforcing bars on the penetration process [23,24]. Luk and Forrestal [13,22] considered that reinforcing bars prevented the radial crack expansion of concrete, however, neglected the penetration resistance. Nevertheless, compared with experiments, the results predicted by this model could produce a difference up to 20%. Riera [25] suggested that the reinforcing bars mainly contribute to improving tensile strength and thus the ballistic limit, even though such improvement was not reflected in the formulas. Dancygier [26] further proposed a model that quantitatively described the effect of reinforcing bars on the penetration resistance by using a reinforcement ratio. Chen et al. [24] considered the reinforcement ratio and tensile strength of the reinforcing bars in their proposed model describing projectile penetration into reinforced concrete.

Currently, most experiments on projectile perforation of reinforced concrete slabs focus on the residual velocity and the ballistic limit for a given slab [5,16,22,25–29,7], under the perforation of a projectile with normal incidence to the slab. For most experiments, the initial impact kinetic energy of the projectile is limited. Namely, the initial impact velocity is low for large projectile masses, while the initial impact velocity is high for small projectile masses. Few experiments have been reported for the scenario of a high-speed projectile with large projectile mass. Moreover, most slabs tested were small and thin [8,6]. Few experimental studies focus on the height of the rear crater or on oblique perforation, which is more likely in reality. The existing relatively successful theoretical perforation models are limited to the scenario of concrete slabs with normal perforation [3,10,13,14,19], and these models are only concerned with the ballistic limit or residual velocity. Very few theoretical analyses have been conducted on the damage of the rear face of concrete slabs or their oblique perforation [9,7]. Chen et al. [24] performed an analytical investigation on the calculation of the residual thickness of normally perforated slabs impact by a rigid projectile under the ballistic limit. However, the prediction had large differences compared with the experimental results. Therefore, a reliable and effective theoretical model for reinforced concrete slabs under oblique projectile penetration has yet to be developed.

In this study, an theoretical model is developed to obtain the failure characteristics of reinforced concrete slabs under impact loading. The process of a rigid projectile perforation of a reinforced concrete slab is divided into three stages, namely initial cratering, tunneling and shear plugging that is consistent with Ref. [21], to enable calculation of the total energy dissipated in the entire process. The energy dissipation of the initial cratering and tunneling stages are calculated by integrating the force displacement curve according to the dynamic cavity expansion theory, where the force is the sum of all the axial resistance forces along the projectile axis. The energy dissipation of shear plugging was then calculated by a newly proposed method considering the effect of reinforcing bars, including the reinforcement ratio and tensile strength of the reinforcing bars. Thus, analytical expressions of the failure characteristics of a reinforced concrete slab are obtained based on energy conservation and the principle of minimum potential energy. Simplified scenarios of the failure characteristics of a rigid projectile oblique perforation of a reinforced concrete slab are discussed. Furthermore, an analytical model for the failure characteristics of a rigid projectile oblique perforation of a concrete slab, a rigid projectile normal perforation of a reinforced concrete slab and a rigid projectile normal perforation of a concrete slab are developed. Experimental results are reported for projectile perforation of thick concrete and reinforced concrete slabs, where the magnitude of damage was measured, including the thickness of the initial and rear cratering, and the length of tunneling. Finally, the predicted results are compared with the experimental data to verify the validity of the present model, followed by discussions on the effects of key model parameters, i.e., impact velocity, concrete compressive strength and reinforcement ratio, on the failure characteristics of a rigid projectile perforation of a reinforced concrete slab.

2. Analytical model

Considering a rigid projectile with a weight of M and a diameter of d perforates a reinforced concrete slab (of thickness h) at an initial oblique angle η and velocity V_0. Recht and Ispon [27,28] suggested that the angle directional change is assumed to occur only in the initial cratering stage due to the action of asymmetric resistance. After the initial cratering stage, the projectile continues to penetrate the reinforced concrete slab with a fixed angle and deflection does not occur in the subsequent process. Fig. 1 shows the general three-stage model [21] which is adopted herein for the perforation of a concrete slab by a rigid projectile. In the cratering stage, the projectile rotates, as well as penetrates into the target. The total angular change at the end of the initial cratering stage is denoted as δ_{max}, and the thickness of initial cratering is kd,where k is a numerical value. Next, in the tunneling stage the projectile translates in a straight line with a fixed angle, and the

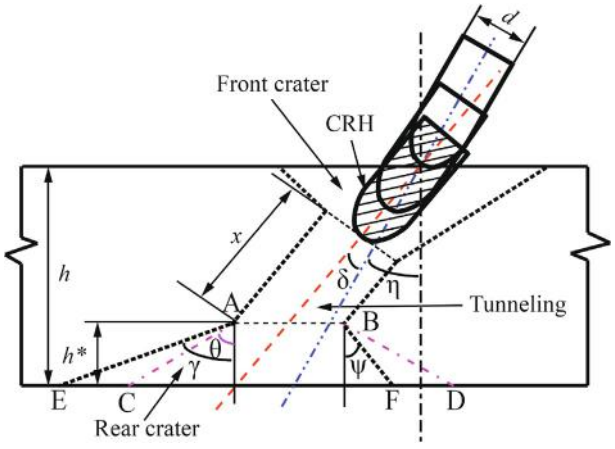

Fig. 1. Three-stages of perforation of a thick concrete slab under oblique projectile impact.

tunneling diameter is consistent with that of the projectile. Finally, the projectile enters the shear plugging stage. In this stage, a shear plugging S_{ABEF}(thickness h^*) forms due to the shearing action of the projectile on the concrete slab; the conical semi-angle on the left and right is defined by γ and ψ, respectively. The shear plugging S_{ABCD} is for the special scenario of normal perforation, and its semi-angle is θ. The value of θ[29–31] increases with the ratio of compressive to tensile strength f_c/f_t. For plain concrete slabs the value of θ is usually around 60°. For the perforation of a reinforced concrete slabs by a rigid projectile, the value of θ and the residual thickness (the height of the shear plugging) will slightly increase and decrease, respectively, with increasing reinforcement ratio and concrete compressive strength. The tunneling stage will be absent when h is reduced to a certain value, and the initial cratering stage will be immediately followed by the shear plugging stage [7]. Hence, for thin slabs the perforation is divided into two-stages, as shown in Fig. 2.

Projectile perforation of reinforced concrete slabs at oblique or normal impact is a complicated nonlinear transient dynamic problem involving high pressure, high strain rate and large deformation [32]. Concrete is a heterogeneous composite material with high porosity, and several microcracks exist in its coarse aggregate and mortar interface. These multi-scale properties have serious influence on the mechanical properties of concrete. For reinforced concrete its mechanical properties are even more complex, because of the addition of reinforcing bars. Therefore, it is difficult to accurately solve this problem using an analytical method as for the perforation of metal material. Therefore, certain assumptions are made to simplify this problem and to effectively analyze the failure characteristics of reinforced concrete slabs subjected to projectile impact loading, as presented below:

(1) All material models satisfy the continuum mechanics assumption;
(2) The deformation of the projectile does not occur during penetration, i.e., the projectile is rigid;
(3) The energy dissipations associated with the following processes are neglected: heat release during the penetration process and the energy dissipations due to friction between materials.
(4) Concrete is a brittle material with low tensile strength [33], this causes the tensile stress wave generated by the stress wave to be reflected on the rear face of the concrete slab and to easily crush the concrete. Thus, the concrete fragments provide little resistance to projectile penetration;
(5) The anti-penetration effect of reinforcing bars only play a role in the shear plugging stage and there is no interaction among the bars and the shear plugging [24].;

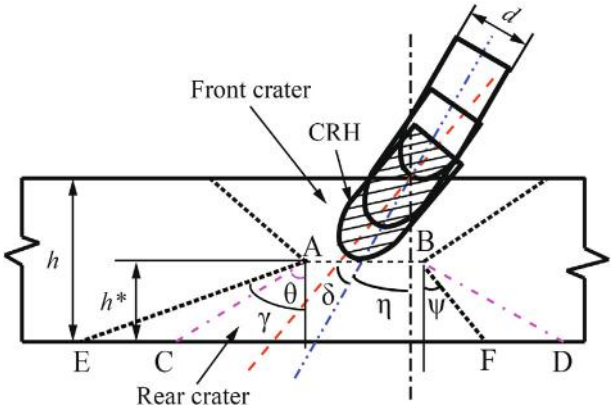

Fig. 2. Two-stages of perforation of a thin concrete slab under oblique projectile impact.

(6) The angle directional change is assumed to occur only in the initial cratering stage due to the action of asymmetric resistance [27,28]. In other stages, the projectile penetrates with a fixed angle, and no deflection occurs in the process;
(7) The residual thickness is determined by the velocity component perpendicular to the slab. The horizontal component only changes the movement of the shear plugging.

2.1. Energy dissipation at each stage

The energy dissipation in the perforation process includes the energy dissipation at the initial cratering stage, tunneling stage and shear plugging stage. The energy dissipation of initial cratering stage, E_1, is the work done by the axial resistance forces on the projectile nose during the initial cratering stage; the energy dissipation of tunneling stage, E_2, is the work done by the axial resistance forces on the projectile nose during tunneling; and the energy dissipation of shear plugging stage, E_3, includes the shear plugging formation E_{3C}, tensile deformation of the reinforcing bars E_{3R}, and the kinetic energy of the shear plugging E_{3P}. Therefore, the total energy dissipation during a projectile perforation of a reinforced concrete slab can be expressed as

$$E = E_1 + E_2 + E_3 \tag{1}$$

where E_2 is zero for the two-stage scenario in which h reduces to a certain value. E_{3P} is equal to zero for the ballistic limit scenario. For the perforation scenario, E_{3P} can be calculated using the velocity v_b and mass m_b of the shear plugging.

$$E_{3P} = \frac{1}{2} m_b v_b^2 \tag{2}$$

where the mass of the shear plugging can be obtained from its the geometry.

$$m_b = \pi \rho h^* \left[3d^2 + 3dh^*(\tan\gamma + \tan\psi) + 2h^{*2}(\tan^2\gamma + \tan^2\psi)\right] \tag{3}$$

2.2. Initial cratering stage

Traditionally, the study of projectile penetration into concrete slabs has been divided into three areas of analysis: the destruction area, the plastic deformation area and the elastic deformation area. Most analysis methods were developed for solving the stresses at the boundary of different areas without involving energy dissipation [11,13,14,19–21]. However, from the perspective of energy dissipation, during a projectile's penetration of concrete, the energy dissipation occurs in the destruction and plastic deformation areas. The elastic strain energy is negligible compared with the energy in the other two areas; and the elastic unloading would make the problem more complicated. Hence, elastic strain energy is ignored during the energy dissipation analysis. In spite of this, it is also extremely difficult to directly obtain the energy dissipation of concrete in the destruction and plastic deformation areas. However, according to the work-energy principle the energy dissipation of the concrete is equivalent to the work done by the axial resistance of the projectile in this stage.

For a penetration depth x, the angle directional change is expressed as δ, and the penetration depth along the projectile axial direction is $x/\cos(\eta+\delta)$. The axial resistance force can be obtained according to the dynamic cavity expansion theory during the initial cratering stage [34]. Integrating the axial resistance force along the penetration axial direction yields E_1:

$$\begin{cases} E_1 = \int_0^{\delta}\int_0^{x} c\frac{x}{\cos(\eta+\delta)}\left(\frac{1}{\cos(\eta+\delta)}dx + \frac{x\sin(\eta+\delta)}{\cos^2(\eta+\delta)}d\delta\right), & x \in [0, kd] \quad (a) \\ E_1 = \int_0^{\delta}\int_0^{kd} c\frac{x}{\cos(\eta+\delta)}\left(\frac{1}{\cos(\eta+\delta)}dx + \frac{x\sin(\eta+\delta)}{\cos^2(\eta+\delta)}d\delta\right), & x \in (kd, +\infty) \quad (b) \end{cases} \tag{4}$$

where c is the resistance constant, given by Ref. [34]:

$$c = \frac{\pi d}{4k}\frac{\left(N^*\rho V_0^2 + Sf_c\right)}{\left(1+\left(\pi k d^3/4m\right)N^*\rho\right)} \tag{5}$$

where ρ is the density of concrete, f_c is the unconfined concrete compressive strength, and k is a dimensionless parameter related to the diameter of the projectile d and the length of the projectile nose l. The value of k can be calculated using the expression $k = (0.707 + l/d)$ according to the slip-line field theory [20]. In Eq. (5), the relationship between S and f_c is described in detailed Refs. [15,34,35], and N^* is the nose shape factor which is described in Refs. [15,19].

The energy dissipation in the first stage can be difficult to solve because of the angle of directional change. However, its value must take on a value between $E_1 = \frac{1}{2}\frac{cx^2}{\cos^2\eta}$ and $E_1 = \frac{1}{2}\frac{cx^2}{\cos^2(\eta+\delta_{\max})}, x \in [0, kd]$, or between $E_1 = \frac{1}{2}\frac{c(kd)^2}{\cos^2\eta}$ and $E_1 = \frac{1}{2}\frac{c(kd)^2}{\cos^2(\eta+\delta_{\max})}, x \in (kd, +\infty)$. An intermediate value is adopted in this study to simplify calculations.

$$\begin{cases} E_1 = \frac{1}{2}\frac{cx^2}{\cos^2(\eta+0.5\delta_{\max})}, & x \in [0, kd] \quad \text{(a)} \\ E_1 = \frac{1}{2}\frac{c(kd)^2}{\cos^2(\eta+0.5\delta_{\max})}, & x \in (kd, +\infty) \quad \text{(b)} \end{cases} \tag{6}$$

where the angle of directional $\delta_{\max}$ can be obtained using the kinetic energy consumption normal to the submerging path [21].

$$\begin{cases} \delta_{\max} = \sin\eta\left(1-\frac{V_r}{V_0}\right)^2, & x \in [0, kd] \quad \text{(a)} \\ \delta_{\max} = \frac{k\pi\sin\eta d^3 Sf_c}{4mV_0^2}, & x \in (kd, +\infty) \quad \text{(b)} \end{cases} \tag{7}$$

where V_r is the residual velocity.

2.3. Tunneling stage

The calculation of energy dissipation for the tunneling stage is similar to that for the initial cratering stage. Based on the energy balance principle, the energy dissipation of concrete is equivalent to the work done by the axial resistance of the projectile in this stage. According to the dynamic cavity expansion theory [34], the axial resistance force during the tunneling stage can be calculated.

$$\sigma_r = A\tau + B\rho_0 V^2 \tag{8}$$

where A and B are only related to the material properties of the slab [18]. In Ref. [13], $A\tau = Sf_c$ and $B = 1$ were adopted for concrete material. Thus, the axial resistance force [13] is given by

$$F = \frac{\pi d^2}{4}\left(S f_c + N^*\rho V_1^2\right) \tag{9}$$

Integrating the axial resistance force along the projectile axial direction gives the energy dissipation in the second stage.

$$\begin{cases} E_2 = 0, & x \in [0, kd] \quad \text{(a)} \\ E_2 = \int_{kd}^{\frac{h-h^*}{\cos(\eta+\delta)}} \frac{\pi d^2}{4}\left(S f_c + N^*\rho V_1^2\right), & x \in (kd, +\infty) \quad \text{(b)} \end{cases} \tag{10}$$

2.4. Shear plugging stage

Based on assumption (5), the energy dissipation of shear plugging stage includes the shear plugging formation, tensile deformation of the reinforcing bars and the kinetic energy of the shear plugging. The failure stress of concrete during pure shear is $\tau_f = f_c/\sqrt{3}$ which is adopted in Ref. [24]. The main reason for choosing this failure criterion is that the process of shear plugging is very complex. Consideration of a more elaborate fracture criterion would make the model much more complicated and difficult to solve. The separation process between the shear plugging and the concrete slab is shown in Fig. 3. According to assumption (7), the residual thickness $(h^* - \omega)$ is caused by the velocity component perpendicular to the slab; and the left and right horizontal displacement of the shear plugging is caused by the horizontal velocity component. Hence, they should hence satisfy the geometric relationship of velocity decomposition during the shear plugging stage:

$$L_{EC} = L_{DF} = (h^* - \omega)\tan\lambda \tag{11}$$

where $\lambda = \frac{\pi}{2} - \eta - \delta$.

Karthik and Mander [36] obtained the failure strain of a reinforced concrete slab under impact loading:

$$\epsilon_f = 0.004 + 5\epsilon_{cc} \tag{12}$$

where ϵ_{cc} is the maximum value of strain in the reinforced concrete slab, and its value can be obtained from the peak concrete strain ϵ_{c0}. The equations are $\epsilon_{cc} = \epsilon_{c0}[1 + 5(K_c - 1)]$ and $\epsilon_{c0} = 0.0015 + f_c(\text{MPa})/70000$, in which K_c is a confinement ratio related to the diameter and arrangement of the reinforcing bars and the value of K_c is equal to 0 and 1.1 for concrete and reinforced concrete slabs, respectively.

It is assumed that the limit compressed displacement during the separation process between the shear plugging and the concrete slab is equivalent to the failure displacement of the shear plugging $\omega_{\max}$.

$$\omega_{\max} = \epsilon_f h^* \tag{13}$$

The energy dissipation of concrete during shear plugging is divided into two parts: the energy dissipation of the left section E_{3C1} and right section E_{3C2}, whose shapes are described by the semi-oval convex platforms $S_{AOO'E}$ and $S_{OBFO'}$, respectively.

The circumference of the upper and lower surfaces of left section can be obtained by the geometric shape of the shear plugging. The lateral surface area of the left section can be approximated as the product of the center line length and generatrix length. The expression of the center line length of the left section is:

$$l_{cL} = \frac{1}{2}[\pi(d + h^*\tan\theta + \omega\tan\theta) + 2(h^* - \omega)\tan\lambda] \tag{14}$$

Thus, the energy dissipation of the left section, E_{3C1}, is given by

$$E_{3C1} = \frac{1}{2}\int_0^{\omega_{\max}} \tau_f l_{cL}\frac{h^* - \omega}{\cos\gamma}\frac{d\omega}{\cos\gamma} \tag{15}$$

Similarly, the lateral surface area of the right section can be approximated as the product of the center line length and the generatrix length. The expression for the center line length of the right section is:

$$l_{cR} = \frac{1}{2}[\pi(d + h^*\tan\theta + \omega\tan\theta) + (2 - \pi)(h^* - \omega)\tan\lambda] \tag{16}$$

Thus, the energy dissipation of the right section, E_{3C2}, is given by

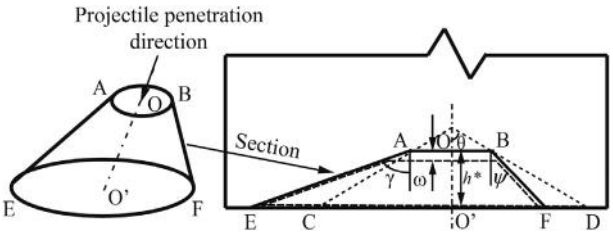

Fig. 3. The separation process between the shear plugging and concrete slab.

$$E_{3C2}=\frac{1}{2}\int_0^{\omega_{\max}}\tau_f l_{cR}\frac{h^*-\omega}{\cos\psi}\frac{d\omega}{\cos\psi} \tag{17}$$

The equivalent stress parameters of shear plugging surface of the left-side $\tau_L=\frac{\pi f_c}{\sqrt{3}\cos^2\gamma}$ and right-side $\tau_R=\frac{\pi f_c}{\sqrt{3}\cos^2\psi}$, the dimensionless parameters $I=\epsilon_f\tan\theta-\frac{1}{3}\tan\theta\epsilon_f^3, J=(\frac{1}{3}\epsilon_f^3-\epsilon_f^2+\epsilon_f)\tan\lambda$, and the length parameter $B=(d\epsilon_f-\frac{1}{2}d\epsilon_f^2)$ are defined to simplify the above complicated equations. Eqs. (15) and (17) leads to the energy dissipation of concrete during the shear plugging:

$$\begin{aligned}E_{3C}&=E_{3C1}+E_{3C2}\\&=\frac{1}{2}B(\tau_L+\tau_R)+\frac{1}{2}\left[I(\tau_L+\tau_R)+J\left(\frac{2\tau_L+(2-\pi)\tau_R}{\pi}\right)\right]h^{*3}\end{aligned} \tag{18}$$

The angles γ and ψ can be obtained by the following method. The left horizontal displacement of shear plugging is divided into two parts:

$$L_{O'E}=L_{EC}+L_{CO'} \tag{19}$$

where $L_{O'E}$ and $L_{CO'}$ can be obtained by the geometric relationship of the shear plugging.

Substituting Eqs. (11) into Eqs. (19) gives

$$(h^*-\omega)\tan\gamma=(h^*-\omega)\tan\lambda+(h^*-\omega)\tan\theta \tag{20}$$

Thus, $\gamma=\arctan(\tan\lambda+\tan\theta)$ can be obtained by Eq. (20).

Similarly, for the right horizontal displacement of the shear plugging, the following can be obtained:

$$L_{O'F}=L_{O'D}-L_{DF} \tag{21}$$

where $L_{O'D}$ and L_{DF} can be obtained by the geometric relationship of the shear plugging.

Substituting Eqs. (11) into Eq. (21) gives

$$(h^*-\omega)\tan\psi=(h^*-\omega)\tan\theta-(h^*-\omega)\tan\lambda \tag{22}$$

Thus, $\psi=\arctan(\tan\theta-\tan\lambda)$ can be obtained by Eq. (22).

The calculation process of the tensile failure energy of the reinforcing bars E_{3R} is similar to that of the energy dissipation of the shear plugging formation. Chen et al. [24] gave the reinforcing bars tensile failure force. Based on this, the reinforcing bars tensile failure force of the left and right section can be expressed as:

$$\begin{cases}F_{sL}=P_L h\rho_s f_s\sin\gamma & (a)\\ F_{sR}=P_R h\rho_s f_s\sin\psi & (b)\end{cases} \tag{23}$$

where ρ_s and f_s is the reinforcement ratio and the tensile strength of the reinforcing bars,respectively. P_L and P_R are the circumference of the middle slice surface of the left and right sections, respectively:

$$\begin{cases}P_L=\frac{1}{2}[\pi(d+h^*\tan\theta)+2h^*\tan\lambda] & (a)\\ P_R=\frac{1}{2}[\pi(d+h^*\tan\theta)+(2-\pi)h^*\tan\lambda] & (b)\end{cases} \tag{24}$$

Based on assumption (5), the tensile failure energy of reinforcing bars E_{RL} and E_{RR} can be obtained by combining the failure strain of the reinforced concrete structure in Eq. (12) and the relationship between the limit displacement and failure strain in Eq. (13):

$$\begin{cases}E_{RL}=\int_0^{\omega_{\max}}F_{sL}d\omega=\int_0^{\varepsilon_f h^*}P_L h\rho_s f_s\sin\gamma d\omega & (a)\\ E_{RR}=\int_0^{\omega_{\max}}F_{sR}d\omega=\int_0^{\varepsilon_f h^*}P_R h\rho_s f_s\sin\psi d\omega & (b)\end{cases} \tag{25}$$

To simplify the expression of the tensile failure energy of reinforcing bars, an influencing parameter, $Q=\pi H\rho_s f_s\varepsilon_f$, is defined for the effect of reinforcing bars. Thus, E_{3R} can be expressed as

$$\begin{aligned}E_{3R}=\;&E_{RL}+E_{RR}=\tfrac{1}{2}Qd(\sin\gamma+\sin\psi)h^*+\\&\tfrac{1}{2}Q\left[\tan\theta(\sin\gamma+\sin\psi)+\tan\lambda\left(\tfrac{2}{\pi}\sin\gamma+\tfrac{2-\pi}{\pi}\sin\psi\right)\right]h^{*2}\end{aligned} \tag{26}$$

An equivalent resistance constant $c_1=\frac{c}{\cos^2(\eta+0.5\delta_{\max})}$, for oblique penetration, and a penetration parameter, $P=\frac{\pi d^2}{4}\left(Sf_c+N^*\rho V_1^2\right)$, for the tunneling stage, are defined. Substituting Eqs. (2), (3), (6), (10), (18), and (26) into Eq. (1), we can obtain the total energy dissipation of oblique perforation process.

2.5. Oblique perforation of a concrete slab

For the scenario of a projectile oblique perforation of a concrete slab, $\rho_s=0$ and $Q=0$. The total energy dissipation of oblique perforation of a concrete slab can be simplified to

$$\begin{cases}E=\;&\frac{1}{2}c_1(h-h^*)^2+\frac{1}{2}B[\tau_L+\tau_R]h^{*2}\\&+\frac{1}{2}\left[I(\tau_L+\tau_R)+J\left(\frac{2\tau_L+(2-\pi)\tau_R}{\pi}\right)\right]h^{*3}\\&+\frac{1}{2}m_b V_b^2, & x\in[0,kd] \quad (a)\\ E=\;&\frac{1}{2}c_1k^2d^2+P\left(\frac{h}{\cos(\eta+\delta)}-\frac{h^*}{\cos(\eta+\delta)}-kd\right)\\&+\frac{1}{2}\left[I(\tau_L+\tau_R)+J\left(\frac{2\tau_L+(2-\pi)\tau_R}{\pi}\right)\right]h^{*3}\\&+\frac{1}{2}B[\tau_L+\tau_R]h^{*2}+\frac{1}{2}m_b V_b^2, & x\in(kd,+\infty) \quad (b)\end{cases} \tag{27}$$

2.6. Normal perforation of a reinforced concrete slab

For the scenario of a projectile normal perforation of a reinforced concrete slab, the initial oblique angle and angular directional change are both equal to zero, namely $\eta=0$ and $\delta=0$. The velocity component in the horizontal direction is also set to zero, meaning the shape of the horizontal direction of the shear plugging is axi-symmetrical, i.e., $\gamma=\psi=\theta$. The equivalent stress parameters of the shear plugging surface for the left-side and right-side are considered to be equal, i.e., $\tau_L=\tau_R=\frac{\pi f_c}{\sqrt{3}\cos^2\theta}$. The equivalent resistance constant c_1 is set equal to c. The term $\tan\lambda$ and the dimensionless parameter J are both set to zero. Therefore, the total energy dissipation of this scenario can be expressed as

$$\begin{cases}E=\;&\frac{1}{2}c(h-h^*)^2+I\tau_L h^{*3}+\frac{1}{2}m_b V_b^2+Qd\sin\theta h^*\\&+(B\tau_L+Q\sin\theta\tan\theta)h^{*2}, & x\in[0,kd] \quad (a)\\ E=\;&\frac{1}{2}ck^2d^2+P(h-h^*-kd)+I\tau_L h^{*3}\\&+(B\tau_L+Q\sin\theta\tan\theta)h^{*2}+Qd\sin\theta h^*\\&+\frac{1}{2}m_b V_b^2, & x\in(kd,+\infty) \quad (b)\end{cases} \tag{28}$$

2.7. Normal perforation of a concrete slab

For the scenario of a projectile normal perforation of a concrete slab, the reinforcement ratio and reinforcing bars influencing parameters are set to zero, i.e., $\rho_s=0$ and $Q=0$. Therefore, the total energy dissipation of this scenario can be expressed as

$$\begin{cases}E=\;&\frac{1}{2}c(h-h^*)^2+I\tau_L h^{*3}+B\tau_L h^{*2}\\&+\frac{1}{2}m_b V_b^2, & x\in[0,kd] \quad (a)\\ E=\;&\frac{1}{2}ck^2d^2+P(h-h^*-kd)\\&+I\tau_L h^{*3}+B\tau_L h^{*2}+\frac{1}{2}m_b V_b^2, & x\in(kd,+\infty) \quad (b)\end{cases} \tag{29}$$

3. Experiments of projectile perforation of thick concrete and reinforced concretes slabs

As stated in the introduction, few experiments have been reported for the scenario of high initial impact velocity for large projectile masses. Moreover, few experimental studies focus on the height of the rear crater. Hence, perforation experiments of thick concrete and reinforced concrete slabs with normal projectile with high velocity ($>$ 1000m/s) were performed for four concrete slabs and four reinforced concrete slabs.

3.1. Projectiles and slabs

Fig. 4 shows the projectile used in the test. The material and geometric parameters of the projectile are shown in Table 1. The size of the concrete slab is 2.0 m $\times$ 2.0 mm $\times$ 1.0 m(in the impact direction), as plotted in Fig. 5. Four layers of reinforcing bars with each layer having 10 bars spaced 200mm apart distributed in the reinforced concrete slab. The mesh size was 200 $\times$ 200 $\times$ 280 mm for the reinforcing bars, as shown in Fig. 6. The densities of the concrete and reinforced concrete slabs were $\rho = 2440\ \mathrm{kg/m^3}$ and $\rho = 2520\ \mathrm{kg/m^3}$, respectively.

When pouring each concrete target, three standard concrete specimens of the same batch were poured separately, with a total of 24. Before the experiment, the compressive strength was tested after 28 days of natural curing which is the same as the targets, and the average value was $f_c = 50.0$ MPa.

3.2. Experimental setup

Fig. 7 shows the schematic view of the experimental setup. Four high-speed cameras were set up to capture the penetration process. Two high-speed cameras were used to capture the destruction process of the front face of the slab and the initial impact velocity with the background panels, which had standard dimension stripes; other two high-speed cameras were used to capture the destruction process on the rear face of the slab.

3.3. Experimental results

The perforation process of the projectile captured by the high-speed cameras is shown in Fig. 8. All the projectiles penetrated into the targets almost perpendicularly, so the values of η are equal to 0 for the present tests. Projectile #1 did not perforate the concrete slab when the impact velocity was 950 m/s. However, a shear plugging was formed on the rear face of the concrete slab and the projectile lodged in the concrete slab, from which it can be inferred that the ballistic limit of the concrete slab is slightly larger than 950 m/s. Specimens #2 and #3 were completely destroyed in the test, so the size of the shear plugging could not be measured. The size of the concrete slab is too small for the velocities exceeding 1400 m/s. Projectiles #5#8 both perforated the reinforced concrete slabs and all slabs were not completely destroyed even if the initial impact velocity was greater than 1400 m/s, which indicates that the reinforcement has a certain anti-penetration effect and can effectively maintain the integrity of the slabs. After perfo-

Fig. 4. Experimental projectile.

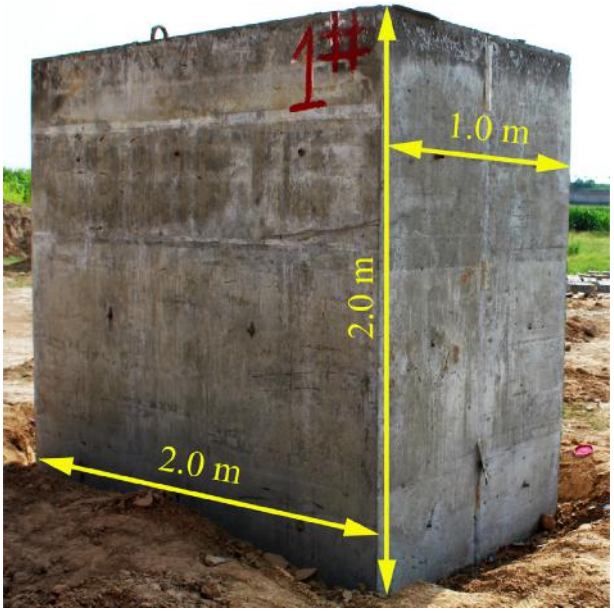

Fig. 5. Concrete slab.

Fig. 6. The layout of the reinforcing bars.

Table 1
Material and geometrical parameters of the projectile.

Material	Yield strength (MPa)	m (kg)	d (m)	CRH	l	k	N^*
7PCrNi3MoV	835.0	9.7	0.1	1.2	0.1	1.707	0.249

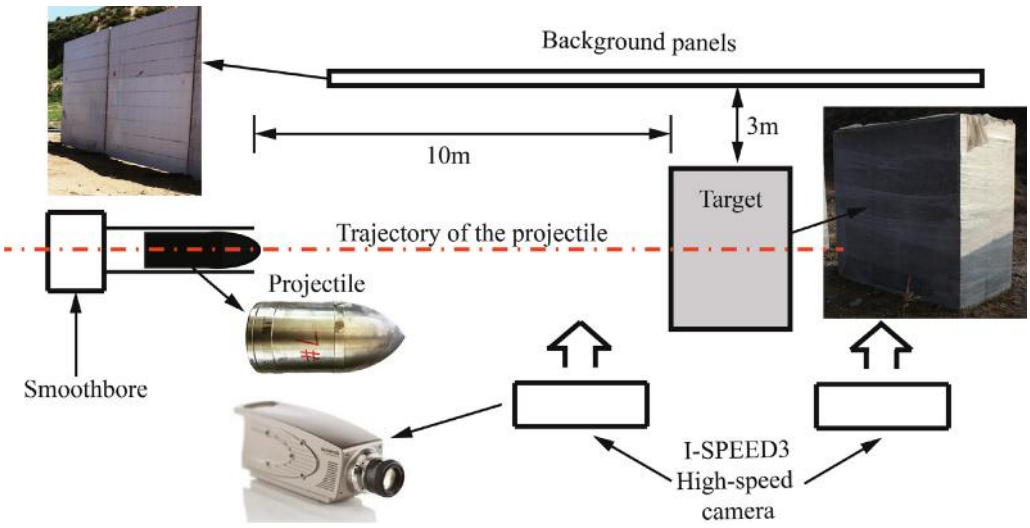

Fig. 7. Schematic view of experimental setup.

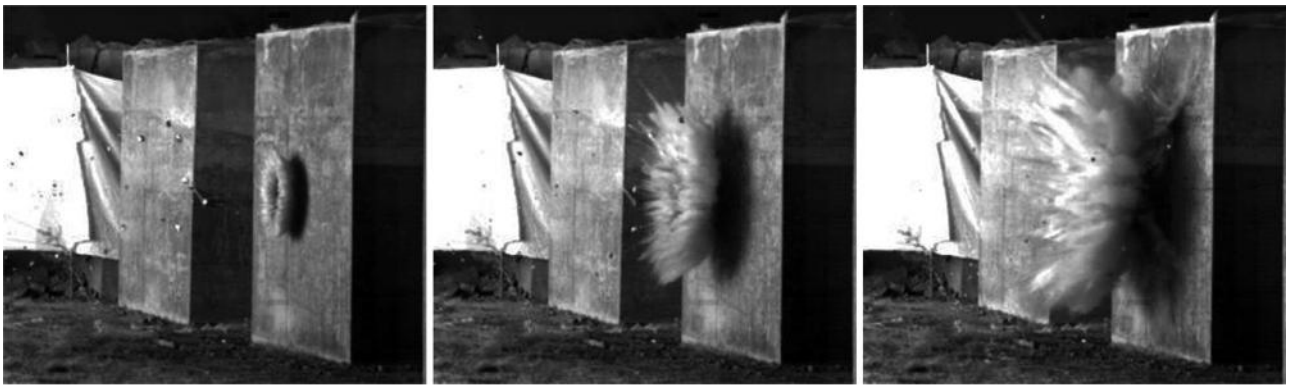

(a) The perforation progress of initial cratering

(b) The perforation progress of shear plugging

Fig. 8. The perforation process of projectile capture by the high-speed cameras.

ration, the slabs showed three stages: initial cratering stage, tunneling stage and shear plugging stage.

Detailed measurements of the slabs are shown in Table 2. A subset of the experimental results is shown in Fig. 9.

4. Results and discussions

The main parameters for evaluating the failure characteristics of a rigid projectile perforation of a reinforced concrete slab are the residual velocity, ballistic limit and residual thickness, which can be obtained by the present method based on energy methods. As stated in the introduction, most experiments tested a single parameter: the ballistic limit or residual velocity, and few experiments tested residual thickness. Therefore, all predictive parameters of the present model, i.e., the residual velocity, ballistic limit, and residual thickness, cannot be simultaneously validated by one set of experimental data. Thus, the residual thickness as a perforation performance parameter is used for verification based on own experiments. The other two parameters are verified using the individual published experimental data.

4.1. Residual thickness

The thickness h^* can be calculated based on the principle of minimum energy

$$\frac{dE}{dh^*} = 0 \tag{30}$$

Assuming that the shear plugging is horizontally ejected after it is separated from the concrete. According to the distribution of concrete fragments behind the slab, the velocity of the shear plugging can be estimated to be about 6 m/s. In this section,the values of η are equal to 0 in the theoretical analyses for the present tests. Furthermore, Table 3 shows the theoretical predictions of residual thickness with different velocities of the shear plugging. For this experimental scenario, the comparisons of the residual thicknesses at different velocities of the shear plugging indicate that the influence of the velocity on the shear plugging is small, with the maximum difference within 10%. Hence, for the scenario with high residual velocity of the projectile and rough engineering calculation, the kinetic energy of the shear plugging can be neglected, greatly simplifying calculation and improving calculation efficiency. In the subsequent analyses presented in this paper, the residual velocity of the shear plugging in the literature could not be obtained, and the previous analysis showed that the influence was small. Therefore, the influence of the kinetic energy of the shear plugging was ignored when compared with other published experimental data.

Specimens #1 to #4 in the experiments presented in Section 3 were concrete slabs. The present model employed $\tan\theta = 2.3$ for concrete slabs according to experimental data. The theoretical results of the residual thickness of concrete slabs obtained by the present model had a good agreement with the experimental data, and the errors are both less than 10.0 % of the experimental data, as shown in Fig. 10.

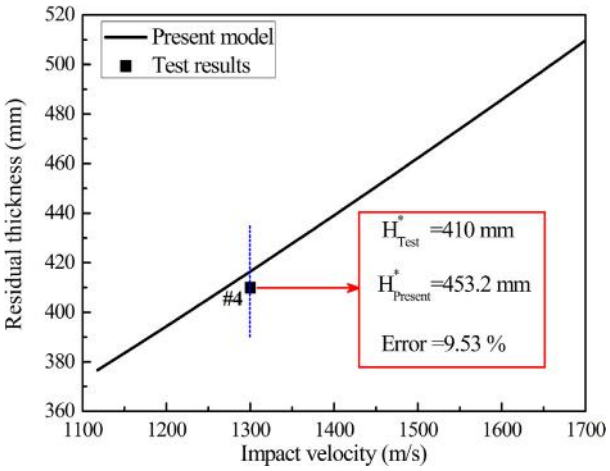

Fig. 10. Comparison of theoretical prediction results of residual thickness of concrete slab with experimental data.

Table 2
Experimental data.

Specimens	Impact velocity (m/s)	Perforated	Open pit depth (mm)	Tunnel length (mm)	Residual thickness (mm)
#1 $\rho_s = 0.0\%$	950	×	305	345	350
#2 $\rho_s = 0.0\%$	1438	✓	–	255	–
#3 $\rho_s = 0.0\%$	1400	✓	–	260	–
#4 $\rho_s = 0.0\%$	1300	✓	310	280	410
#5 $\rho_s = 0.2\%$	1481	✓	290	340	370
#6 $\rho_s = 0.2\%$	1283	✓	300	360	340
#7 $\rho_s = 0.2\%$	1428	✓	310	330	360
#8 $\rho_s = 0.2\%$	1360	✓	300	350	350

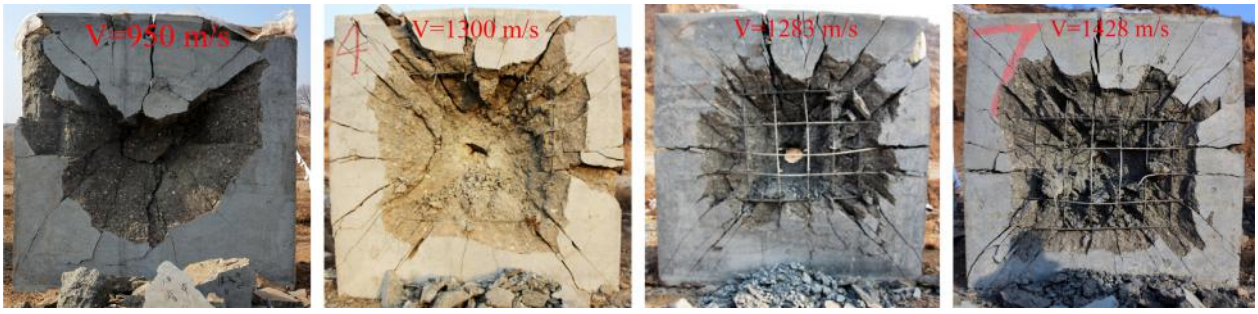

Fig. 9. Typical experimental results of the perforation of concrete and reinforced concrete slabs.

Table 3
The theoretical predictions of residual thickness with different velocities of the shear plugging.

Specimens	Impact velocity (m/s)	Residual thickness (mm)				Maximum difference[a]
		0 m/s	6 m/s	10 m/s	20 m/s	
#4	1300	455.1	453.2	448.5	423.3	6.98%
#5	1481	340.4	338.4	331.9	315.7	7.25%
#6	1283	305.9	302.1	296.9	282.2	7.75%
#7	1428	330.7	327.8	321.4	306.6	7.29%
#8	1360	319.5	318.6	309.8	294.8	7.73%

[a] The maximum difference is defined as the difference between the minimum and maximum prediction.

The residual thickness and ballistic limit of the concrete slab predicted by the present model are 388.3 mm and 1115.0 m/s, respectively. These results are in good agreement with the experimental data of specimens #1 in Section 3.3. The damage area on the rear face of the concrete slab can be calculated by predicting the residual thickness based on the geometry of the shear plugging.

$$D^* = d + 2h^* \tan\theta \tag{31}$$

The residual thickness of the specimens #2 and #3 can be predicted as larger than 2.0 m by the present model, which indicate that the concrete slab is completely destroyed, which is consistent with the experimental results.

Specimens #5 to #8 in the experiments presented in Section 3 were reinforced concrete slabs, in which the reinforcement ratio was $\rho_s = 0.2\%$ and the tensile strength of reinforcing bars was $f_s = 500$ MPa. The present model employed $\tan\theta = 2.5$ for reinforced concrete slabs according to the experimental data. Fig. 11 shows the comparison of theoretical prediction results of residual thickness of reinforced concrete slab with experimental data, and the errors are within 12.0%.

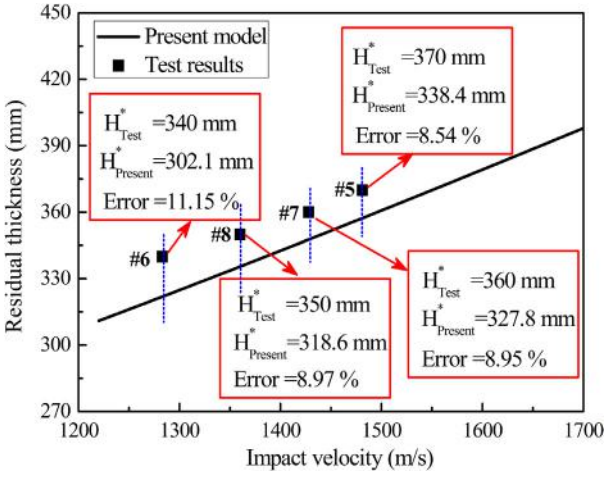

Fig. 11. Comparison of theoretical prediction results of residual thickness of reinforced concrete slab with experimental data.

Table 4
The geometric parameters for the concrete and projectile of Dancygier's tests [26].

ρ (kg/m^3)	m (kg)	d (m)	CRH	l	k	N^*
2300	0.165	0.025	3	0.0421	2.107	0.113

The residual thickness of the reinforced concrete slab predicted by the present model are 313.3 mm and 1195.0 m/s, respectively. The corresponding predicted result by the model of Chen et al. [24] are 90.0 mm and 810.3 m/s, respectively. These results show that the results predicted by the present model agree better with the experimental data than those by Chen et al.s model [24] for the residual thickness. Moreover, the residual thickness is independent of initial impact velocity and determined by the geometric configuration of perforation for the model of Chen et al. [24]. Thus, the residual thickness is a constant for a given projectile and target. In the present model, the residual thickness, which is obtained by the energy method, is related to the initial impact velocity. It indicates that the residual thickness changes with the initial impact velocity, which is more consistent with the actual situation.

4.2. Ballistic limit

The initial velocity and the residual thickness are defined as V_{BL} and h^*_{BL}, respectively, for the ballistic limit scenario. In this scenario, the total energy dissipation will be equal to the kinetic energy of the projectile. Combining with the Eq. (30), V_{BL} and H^*_{BL} can be determined by solving the following:

$$\begin{cases} \frac{1}{2}mV_{BL}^2 - E_{BL} = 0 \\ \frac{dE_{BL}}{dh^*_{BL}} = 0 \end{cases} \tag{32}$$

The ballistic limit of rigid projectiles penetrating reinforced concrete slabs under various reinforcement ratios are reported in Ref. [26]. The geometric parameters for the concrete and projectile are shown in Table 4. All the projectiles penetrate into the targets perpendicularly, so the values of η are equal to 0 for these tests. The half-cone angle of the shear plugging was not mentioned in Dancygiers [26] tests. The present model employed $\tan\theta = 4.0$ based on another test of Dancygiers [8].

The ballistic limit is defined as the condition when the projectile is stuck in the reinforced concrete slab [37], so the ballistic limit is

Table 5
Comparison of theoretical prediction results of ballistic limit with experimental data and the model of Chen et al. [24].

Specimens	Concrete		Reinforcement		Test data (m/s)			Present model	The model of Chen et al. [24]
	H(mm)	f_c(MPa)	ρ_s(%)	f_s(MPa)	Unperforated	Perforation limit		$\tan\theta = 4.0$	
A4-5-R	50	35	0.16	382	140	–	158	177.6	182.5
A3-5-R	50	35	0.36	382	159	165	–	177.72	185.5
A8-5-R	50	39	0.49	316	160	–	–	184.5	192.1
A2-5-R	50	35	0.71	183	209	222	–	177.7	185.2
A7-5-R	50	39	0.92	316	171	–	–	184.8	197.0
A5-5-R	50	39	1.82	534	202	–	221	186.0	217.4
A6-5-R	50	35	1.82	473	–	–	191	179.2	209.5
A4-6-R	60	39	0.12	382	228	–	–	226.6	238.8
A3-6-R	60	35	0.29	382	208	–	224	218.6	234.4
A2-6-R	60	35	0.57	183	–	232	242	218.6	234.1
A5-6-R	60	39	0.46	534	–	–	279	227.0	266.9
A6-6-R	60	35	0.46	473	–	236	248	218.8	257.7
B11-5-R	50	35	0.20	650	–	–	147	177.7	185.2
B12-5-R	50	34	0.20	600	126	–	141	175.9	183.3
B13-5-R	50	35	0.20	450	146	–	219	177.6	183.6
B22-5-R	50	34	0.99	600	181	210	251	176.9	200.2
B51-5-R	50	34	0.15	650	157	–	158	175.9	182.4
B52-5-R	50	34	0.26	600	148	–	159	176.0	184.7
B53-5-R	50	35	0.61	450	158	–	165	178.0	190.7
B55-5-R	50	34	0.61	650	157	162	253	176.5	193.6

difficult to obtained. Hence, most experimental data of ballistic limit tests are around the ballistic limit. Table 5 shows the comparison of theoretical prediction results of ballistic limit with experimental data and Chen et al.s model [24]. The ballistic limit of the theoretical predictions by the present model is mostly within that of the experimental data. The fluctuation range of the ballistic limit predicted by the theoretical model predicts fluctuation range as being smaller than experimentally obtained values; the reason for this is that the theoretical model is ideal and is not interfered with by external factors. The prediction results by the present model are slightly smaller than by the model of Chen et al.s [24]. The difference between the two models is that the plug is separated from the surrounding material as soon as the shear failure criterion is satisfied along the plug surface in Chen et al.'s model [24], but in the present model the plug is separated from the surrounding material with the process of compression and shearing.

4.3. Residual velocity

Combining Eqs. (29) and (30), the total dissipation energy can be obtained. Based on the energy conservation principle, the residual velocity can then be calculated as follows:

$$V_r = \sqrt{V_0^2 - 2E/m} \tag{33}$$

The Protective Technology Research Center at Nanyang Technological University [38] conducted projectile oblique perforation tests of thick concrete slabs with an initial oblique angle of $\eta = 30^\circ$, and measured the residual velocity. The geometric parameters for the concrete and projectile were shown in Table 6. Based on the experimental results, $\tan\theta = 2.60$, was adopted in the present model for the concrete slab.

Fig. 12 shows that the prediction of the projectile residual velocity using the present model agrees well with the experimental data for various thicknesses of concrete slabs. As the thickness of the slab and initial impact velocity increases, the theoretical predictions agree more closely with the experimental data.

Buzaud [39] conducted the tests of projectile oblique perforation of thin concrete slabs with an initial oblique angle of $\eta = 30^\circ$, and measured the residual velocity. The geometric parameters for the concrete and projectile were shown in Table 7. The present model employed $\tan\theta = 3.0$ for concrete slabs according to the experimental data. Fig. 13 shows that the prediction of the residual velocity of thin concrete slabs using the presented model is close to the experimental data.

Comparing the prediction results by the present model and the Chen et al. model [21] shows that the present model prediction of the residual velocity is closer to the experimental data, and the error is slightly smaller than that of the model of Chen et al. [21]. However, when the initial impact velocity of the projectile is slightly higher than the ballistic limit, the predicted result is different from the experimental data. The reason is that the effect of the plug kinetic energy was not considered in the present model.

4.4. Parametric analysis of failure characteristics

Based on the PTRC-NTU tests, the present model is utilized to predict the residual thickness impacted at different initial impact velocities. The initial oblique angle of $\eta = 30^\circ$. Fig. 14 shows that h^* increases with V_0, while the increase rate of h^* decreases with the increase of f_c. It is indicated that the initial impact velocity has a lower influence on the concrete slab with a higher compressive strength. That means that the residual thickness of a concrete slab with low compressive strength is more sensitive to the initial impact velocity.

Fig. 15 shows the theoretical results of the changes in V_{BL} versus f_c for various thicknesses of concrete slabs. V_{BL} increases with increasing f_c, while the increase rate of V_{BL} gradually decrease.

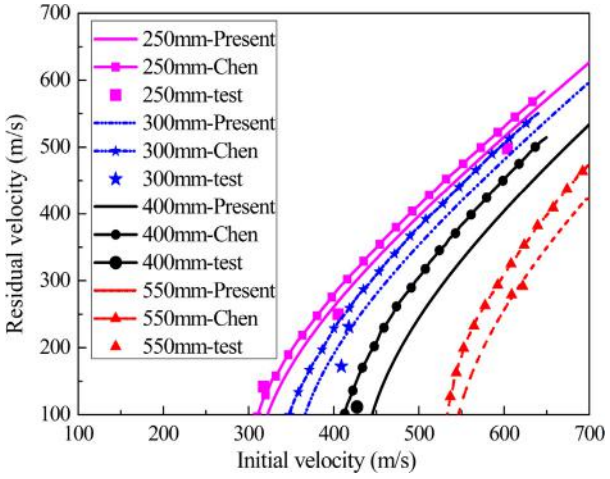

Fig. 12. Predictions of the projectile residual velocity compare with Fans experimental data in various thicknesses of concrete slabs.

Table 7
The geometric parameters for the concrete and projectile of Buzauds tests [39].

ρ (kg/m^3)	h (m)	f_c	m (kg)	d (m)	CRH	l	k
2336	0.60	40.0	79.5	0.16	6.0	0.317	2.69

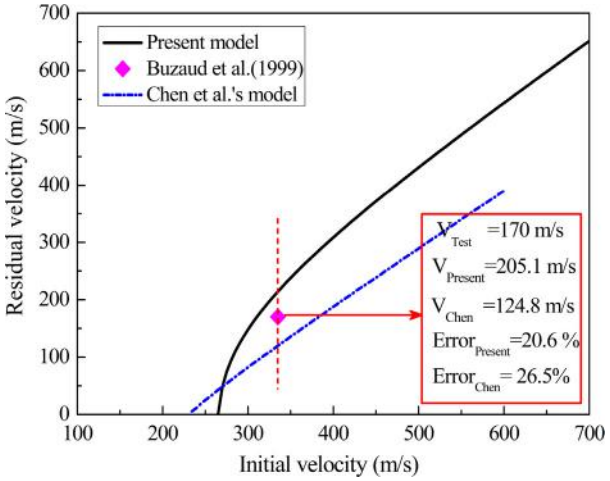

Fig. 13. Predictions of the projectile residual velocity compared with Buzauds experimental data.

Table 6
The geometric parameters for the concrete and projectile of Fans tests [38].

ρ (kg/m^3)	f_c (MPa)	h (m)	m (kg)	d (m)	CRH	l	k
2280	42.0	0.25, 0.30, 0.40, 0.55	0.165	0.025	3.0	0.0421	2.107

Fig. 16 presents the predictions of the changes in h^* with f_c of the concrete slab for different slab thicknesses. The increase of f_c leads to a decrease of h^*. However, the decrease rate of the h^* gradually decreases as f_c increases.

Based on the PTRC-NTU tests, the effect of reinforcing bars was considered, and the corresponding tensile strength was set to $f_s = 500$ MPa . Fig. 17 shows the predictions of the ballistic limit of the slab with different reinforcement ratios. The reinforcement ratio ρ_s has a slight influence on the ballistic limit, which increases almost linearly with the increase of the reinforcement ratio.

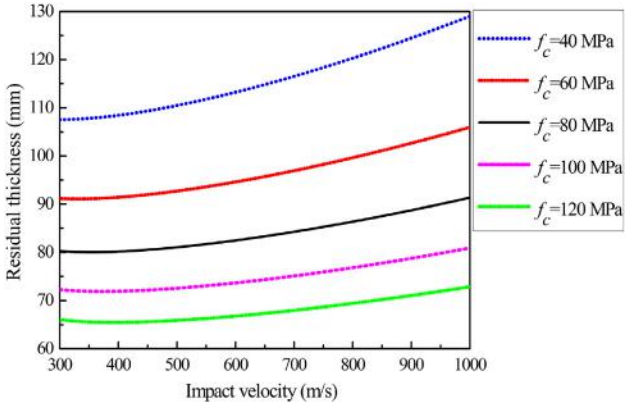

Fig. 14. Relationship between the residual thickness and the initial impact velocity.

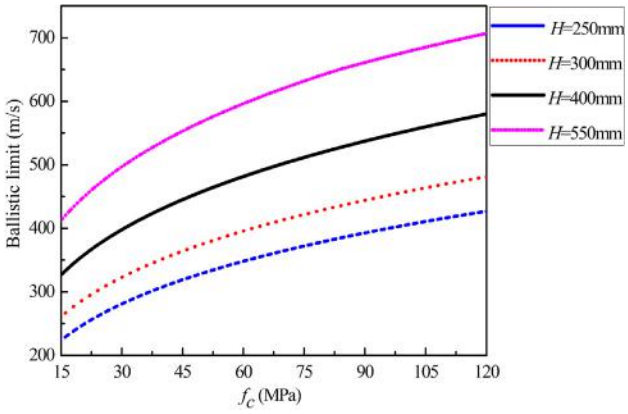

Fig. 15. Relationship between the ballistic limit and the concrete compressive strength.

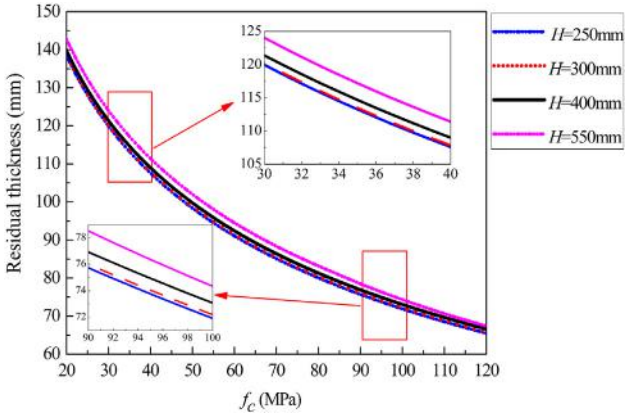

Fig. 16. Relationship between the residual thickness and the concrete compressive strength.

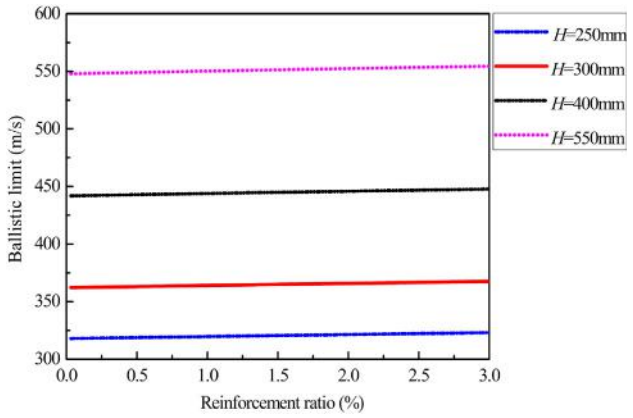

Fig. 17. Relationship between the ballistic limit and the reinforcement ratio.

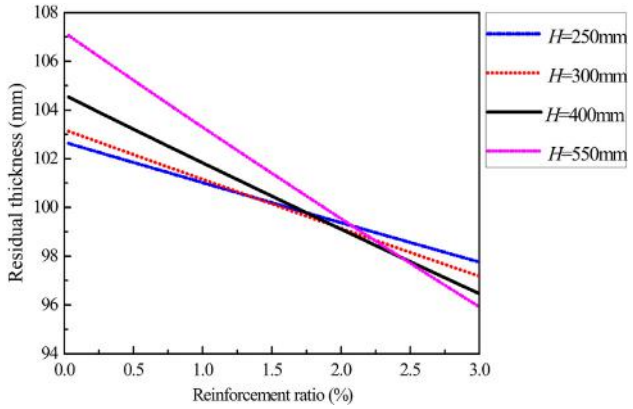

Fig. 18. Relationship between the residual thickness and the reinforcement ratio.

The residual thickness is predicted for the slab with different reinforcement ratios and given in Fig. 18. The reinforcement ratio ρ_s has a slight influence on h^*, and the largest decrease is 11 mm; h^* is almost linearly related with ρ_s. However, the rate of the decrease of h^* increases with the slab thickness, which suggests that the reinforcement ratio has more influence on thick reinforced concrete slabs.

5. Conclusion

The current, relatively successful theoretical models of perforation are limited to concrete slabs with normal perforation, and these models only focus on one penetration parameter: the ballistic limit or residual velocity. Very little theoretical analysis has been performed on the residual thickness of the cone shear or oblique perforation of a reinforced concrete slab.

In this paper, the failure characteristics of a rigid projectile perforation of a reinforced concrete slab have been theoretically investigated. A failure analytical model was constructed to assess the characteristics of a reinforced concrete slab under oblique perforation by a rigid projectile using the energy method. Thus, analytical expressions of failure characteristics (residual thickness, ballistic limit, residual velocity) of a reinforced concrete slab are obtained. Projectile perforation experiments of concrete and reinforced concretes slabs were conducted, and the experimental data were compared with the theoretical model. The results predicted by the theoretical model closely agreed with the experimental data. Fur-

thermore, the effects of key parameters, i.e., the initial impact velocity, concrete compressive strength, and reinforcement ratio, on the failure characteristics of a rigid projectile perforation of a reinforced concrete slab were obtained. Some conclusions are obtained and listed in the following:

(1) The results predicted by the present model closely agreed with the experimental data, indicating that the proposed analytical model based on energy methods was effective in obtaining the failure characteristics of a rigid projectile perforation of a reinforced concrete slab;
(2) The comparison results show that the result predicted by the present model agree better with the experimental data than that predicted by Chen et al.s model for the residual thickness. In the present model, the residual thickness is related to the initial impact velocity, which is more consistent with the actual situation. This proves that the present model, based on energy methods, is reasonable and effective;
(3) The residual thickness and velocity increased with the initial impact velocity, while the increase rate of the residual thickness and velocity are gradually increased and decreased, respectively;
(4) The ballistic limit and residual thickness increased and decreased, respectively, with increasing concrete compressive strength, whereas the corresponding increase and decrease rate both decreased gradually;
(5) The effects of the reinforcement ratio on the perforation performance are much smaller than the initial impact velocity and concrete compressive strength. However, the effect of the reinforcement ratio on thick concrete slabs was more evident than on thin reinforced concrete slabs.

Declaration of Competing Interest

The authors declared that they have no conflicts of interest to this work.

Acknowledgements

This work was supported by the National Natural Science Foundation of China (Grant Nos. 11822203 and 11532012) and the China Postdoctoral Science Foundation (Grant No. 2018M641209).

References

[1] Y. Su, J. Li, C. Wu, P. Wu, Z.-X. Li, Effects of steel fibres on dynamic strength of UHPC, Constr. Build. Mater. 114 (2016) 708–718, https://doi.org/10.1016/j.conbuildmat.2016.04.007. URL: http://www.sciencedirect.com/science/article/pii/S095006181630544X.
[2] T. Almusallam, Y. Al-Salloum, S. Alsayed, R. Iqbal, H. Abbas, Effect of CFRP strengthening on the response of RC slabs to hard projectile impact, Nucl. Eng. Des. 286 (2015) 211–226, https://doi.org/10.1016/j.nucengdes.2015.02.017. URL: http://www.sciencedirect.com/science/article/pii/S0029549315000990.
[3] N.A. Siddiqui, B.M. Khateeb, T.H. Almusallam, H. Abbas, Reliability of double-wall containment against the impact of hard projectiles, Nucl. Eng. Des. 270 (2014) 143–151, https://doi.org/10.1016/j.nucengdes.2014.01.003. URL: http://www.sciencedirect.com/science/article/pii/S0029549314000272.
[4] J. Liu, C. Wu, X. Chen, Numerical study of ultra-high performance concrete under non-deformable projectile penetration, Constr. Build. Mater. 135 (2017) 447–458, https://doi.org/10.1016/j.conbuildmat.2016.12.216. URL: http://www.sciencedirect.com/science/article/pii/S0950061816321493.
[5] Y. Peng, H. Wu, Q. Fang, J. Liu, Z. Gong, Residual velocities of projectiles after normally perforating the thin ultra-high performance steel fiber reinforced concrete slabs, Int. J. Impact Eng. 97 (1–9) (2016), https://doi.org/10.1016/j.ijimpeng.2016.06.006. URL: http://www.sciencedirect.com/science/article/pii/S0734743X16300847.
[6] A. Saarenheimo, M. Tuomala, K. Calonius, Shear punching studies on an impact loaded reinforced concrete slab, Nucl. Eng. Des. 295 (2015) 730–746, https://doi.org/10.1016/j.nucengdes.2015.04.018. URL: http://www.sciencedirect.com/science/article/pii/S0029549315001454.
[7] X. Xu, T. Ma, Z. Wang, A theoretical model of rigid projectile perforation of concrete slabs using the energy method, Sci. China Technol. Sci. 61 (2018) 699–710, https://doi.org/10.1007/s11431-017-9183-1. URLhttps://doi.org/10.1007/s11431-017-9183-1.
[8] A. Dancygier, Rear face damage of normal and high-strength concrete elements caused by hard projectile impact, ACI Struct. J. 95 (1998) 291–304.
[9] X. Xu, T. Ma, J. Ning, Failure mechanism of reinforced concrete subjected to projectile impact loading, Eng. Fail. Anal. 96 (2018), https://doi.org/10.1016/j.engfailanal.2018.11.006.
[10] Q. Li, S. Reid, H. Wen, A. Telford, Local impact effects of hard missiles on concrete targets, Int. J. Impact Eng. 32 (2005) 224–284, https://doi.org/10.1016/j.ijimpeng.2005.04.005. URL: http://www.sciencedirect.com/science/article/pii/S0734743X05000692. fifth International Symposium on Impact Engineering.
[11] W. Goldsmith, Non-ideal projectile impact on targets, Int. J. Impact Eng. 22 (1999) 95–395, https://doi.org/10.1016/S0734-743X(98)00031-1. URL: http://www.sciencedirect.com/science/article/pii/S0734743X98000311.
[12] T.H. Almusallam, N.A. Siddiqui, R.A. Iqbal, H. Abbas, Response of hybrid-fiber reinforced concrete slabs to hard projectile impact, Int. J. Impact Eng. 58 (2013) 17–30. URL: https://doi.org/10.1016/j.ijimpeng.2013.02.005.
[13] M. Forrestal, B. Altman, J. Cargile, S. Hanchak, An empirical equation for penetration depth of ogive-nose projectiles into concrete targets, Int. J. Impact Eng 15 (1994) 395–405, https://doi.org/10.1016/0734-743X(94)80024-4. URL: http://www.sciencedirect.com/science/article/pii/0734743X94800244.
[14] M. Forrestal, D. Frew, J. Hickerson, T. Rohwer, Penetration of concrete targets with deceleration-time measurements, Int. J. Impact Eng. 28 (2003) 479–497, https://doi.org/10.1016/S0734-743X(02)00108-2. URL: http://www.sciencedirect.com/science/article/pii/S0734743X02001082.
[15] M. Forrestal, D. Frew, S. Hanchak, N. Brar, Penetration of grout and concrete targets with ogive-nose steel projectiles, Int. J. Impact Eng 18 (1996) 465–476, https://doi.org/10.1016/0734-743X(95)00048-F. URL: http://www.sciencedirect.com/science/article/pii/0734743X9500048F.
[16] S. Hanchak, M. Forrestal, E. Young, J. Ehrgott, Perforation of concrete slabs with 48 mpa (7 ksi) and 140 mpa (20 ksi) unconfined compressive strengths, Int. J. Impact Eng 12 (1992) 1–7, https://doi.org/10.1016/0734-743X(92)90282-X. URL: http://www.sciencedirect.com/science/article/pii/0734743X9290282X.
[17] D. Frew, M. Forrestal, J. Cargile, The effect of concrete target diameter on projectile deceleration and penetration depth, Int. J. Impact Eng 32 (2006) 1584–1594, https://doi.org/10.1016/j.ijimpeng.2005.01.012. URL: http://www.sciencedirect.com/science/article/pii/S0734743X0500028X.
[18] Y. Xu, L. Keer, V. Luk, Elastic-cracked model for penetration into unreinforced concrete targets with ogival nose projectiles, Int. J. Solids Struct. 34 (1997) 1479–1491, https://doi.org/10.1016/S0020-7683(96)00099-6.
[19] X. Chen, Q. Li, Deep penetration of a non-deformable projectile with different geometrical characteristics, Int. J. Impact Eng. 27 (2002) 619–637, https://doi.org/10.1016/S0734-743X(02)00005-2. URL: http://www.sciencedirect.com/science/article/pii/S0734743X02000052.
[20] Q. Li, X. Chen, Dimensionless formulae for penetration depth of concrete target impacted by a non-deformable projectile, Int. J. Impact Eng 28 (2003) 93–116, https://doi.org/10.1016/S0734-743X(02)00037-4. URL: http://www.sciencedirect.com/science/article/pii/S0734743X02000374.
[21] X. Chen, S. Fan, Q. Li, Oblique and normal perforation of concrete targets by a rigid projectile, Int. J. Impact Eng 30 (2004) 617–637, https://doi.org/10.1016/j.ijimpeng.2003.08.003. URL: http://www.sciencedirect.com/science/article/pii/S0734743X0300099X.
[22] V. Luk, M. Forrestal, Penetration into semi-infinite reinforced-concrete targets with spherical and ogival nose projectiles, Int. J. Impact Eng 6 (1987) 291–301, https://doi.org/10.1016/0734-743X(87)90096-0. URL: http://www.sciencedirect.com/science/article/pii/0734743X87900960.
[23] J. Feng, W. Sun, Z. Liu, C. Cui, X. Wang, An armour-piercing projectile penetration in a double-layered target of ultra-high-performance fiber reinforced concrete and armour steel: experimental and numerical analyses, Mater. Des. 102 (2016) 131–141, https://doi.org/10.1016/j.matdes.2016.04.021. URL: http://www.sciencedirect.com/science/article/pii/S0264127516304889.
[24] X. Chen, X. Li, F. Huang, H. Wu, Y. Chen, Normal perforation of reinforced concrete target by rigid projectile, Int. J. Impact Eng. 35 (2008) 1119–1129, https://doi.org/10.1016/j.ijimpeng.2008.01.002. URL: http://www.sciencedirect.com/science/article/pii/S0734743X08000158, first International Conference on Analysis and Design of Structures Against Explosive and Impact Loads (ADSEI).
[25] J. Riera, Penetration, scabbing and perforation of concrete structures hit by solid missiles, Nucl. Eng. Des. 115 (1989) 121–131, https://doi.org/10.1016/0029-5493(89)90265-3. URL: http://www.sciencedirect.com/science/article/pii/0029549389902653.
[26] A.N. Dancygier, Effect of reinforcement ratio on the resistance of reinforced concrete to hard projectile impact, Nucl. Eng. Des. 172 (1997) 233–245, https://doi.org/10.1016/S0029-5493(97)00055-1. URL: http://www.sciencedirect.com/science/article/pii/S0029549397000551.
[27] R.F. RECHT, T. Ipson, Ballistic perforation dynamics, J. Appl. Mech. 30 (1963) 384–390, https://doi.org/10.1115/1.363656. URL: https://ci.nii.ac.jp/naid/10008225753/en/.
[28] T.W. Ipson, R.F. Recht, Ballistic-penetration resistance and its measurement, Exp. Mech. 15 (1975) 249–257, https://doi.org/10.1007/BF02318057. URL: https://doi.org/10.1007/BF02318057.

[29] A. Dancygier, D. Yankelevsky, High strength concrete response to hard projectile impact, Int. J. Impact Eng. 18 (1996) 583–599, https://doi.org/10.1016/0734-743X(95)00063-G. URL: http://www.sciencedirect.com/science/article/pii/0734743X9500063G.

[30] S. Jones, W.K. Rule, On the optimal nose geometry for a rigid penetrator, including the effects of pressure-dependent friction, Int. J. Impact Eng 24 (2000) 403–415, https://doi.org/10.1016/S0734-743X(99)00157-8. URL: http://www.sciencedirect.com/science/article/pii/S0734743X99001578.

[31] L. Jinzhu, L. Zhongjie, Z. Hongsong, H. Fenglei, Perforation experiments of concrete targets with residual velocity measurements, Int. J. Impact Eng. 57 (2013) 1–6, https://doi.org/10.1016/j.ijimpeng.2013.01.007. URL: http://www.sciencedirect.com/science/article/pii/S0734743X13000146.

[32] Q. Fang, H. Wu, Concrete Structures Under Projectile Impact, Springer, Singapore, Singapore, 2017, pp. 497–558. URL: https://doi.org/10.1007/978-981-10-3620-0_12.

[33] J. Liu, C. Wu, J. Li, Y. Su, X. Chen, Numerical investigation of reactive powder concrete reinforced with steel wire mesh against high-velocity projectile penetration, Constr. Build. Mater. 166 (2018) 855–872, https://doi.org/10.1016/j.conbuildmat.2018.02.001.

[34] M. Forrestal, V. Luk, Penetration into soil targets, Int. J. Impact Eng. 12 (1992) 427–444, https://doi.org/10.1016/0734-743X(92)90167-R. URL: http://www.sciencedirect.com/science/article/pii/0734743X9290167R.

[35] X. Chen, F. Lu, D. Zhang, Penetration trajectory of concrete targets by ogived steel projectile—experiments and simulations, Int. J. Impact Eng. 120 (2018) 202–213, https://doi.org/10.1016/j.ijimpeng.2018.06.004. URL: http://www.sciencedirect.com/science/article/pii/S0734743X18303336.

[36] M. Karthik, J. Mander, Stress-block parameters for unconfined and confined concrete based on a unified stress-strain model, J. Struct. Eng. 137 (2011) 270–273. URL:https://ascelibrary.org/doi/pdf/10.1061/10.1061/(ASCE)ST.1943-541X.0000294.

[37] A. Rajagopal, N.K. Naik, Oblique ballistic impact behavior of composites, Int. J. Damage Mech 23 (2014) 453–482. URL: https://doi.org/10.1177/1056789513499268.10.1177/1056789513499268. arXiv: https://doi.org/10.1177/1056789513499268.

[38] S.C. Fan, X.Q. Zhou, Constitutive model for reinforced concrete against penetration, report, Protective Technology Research Centre, School of Civil and Structural Engineering, Nanyang Technological University, Singapore, 2000.

[39] E. Buzaud, R. Laurensou, A. Darrigadeet, Hard target defeat: an analysis of reinforced concrete perforation process, in: The 9th International Symposium on Interaction of the Effects of Munitions with Structures, vol. 3–7, 1999, pp. 283–290..